IEEE Access
Multidisciplinary | Rapid Review | Open Access Journal

IEEE POWER & ENERGY SOCIETY SECTION

Received January 5, 2022, accepted January 19, 2022, date of publication February 7, 2022, date of current version February 18, 2022.

Digital Object Identifier 10.1109/ACCESS.2022.3149273

RoCoF-Minimizing H_2 Norm Control Strategy for Multi-Wind Turbine Synthetic Inertia

ESTEBAN RIQUELME, HECTOR CHAVEZ, (Member, IEEE), AND KARINA ACOSTA BARBOSA, (Senior Member, IEEE)
Electrical Engineering Department, University of Santiago, Santiago 3519, Chile

Corresponding author: Esteban Riquelme (esteban.riquelme@usach.cl)

This work was supported by the Agencia Nacional de Investigacion y Desarrollo (ANID)/Fondo Nacional de Desarrollo Cientifico y Tecnologico Fondecyt, Chile, under Grant 1191302. The work of Esteban Riquelme was supported by the ANID/Scholarship Program/DOCTORADO/2019.

ABSTRACT The reduction in system inertia under the penetration of power electronic-interfaced generation has fostered various proposals on wind synthetic inertia. Several works in the state of the art propose control strategies to optimize synthetic inertia performance; however, most of the performance metrics indirectly represent frequency control adequacy indicators such as rate of change of frequency or frequency nadir. Also, control definitions assume that there is one variable speed wind turbine and one controller, which limits the applicability of the proposals as power systems normally count with various wind turbines/farms over extended geographical areas with different wind regimes. This work presents a H_2 optimal control approach for a variable speed wind turbine synthetic inertia controller. First, the objective of the formulation is to explicitly minimize the rate of change of power system frequency. Second, a stability proof for the multi-wind turbine case is proposed, allowing optimal controllers to be independently implemented for an arbitrary number of wind turbines and wind regimes. The effectiveness of the proposed control scheme is demonstrated with a numerical example, considering an empirically-validated, reduced-order model of the Electric Reliability Council of Texas frequency dynamics.

INDEX TERMS Frequency control, optimal control, synthetic inertia, wind farm, frequency response.

I. INTRODUCTION

The inertia and frequency response reduction in power systems has led to various approaches of Variable Speed Wind Turbine (VSWT) Synthetic Inertia (SI) [1]. Most of these approaches normally consist in withdrawing kinetic energy from the moving part of the turbine, emulating the behavior of synchronous machines. In general, the turbine kinetic energy must be restored afterwards to reestablish the operating speed given by maximum power point tracking controllers, leading to different control proposals aiming to maintain SI stability. Most approaches consider full control of electric torque, so methods require the use of type III (doubly fed induction generator) or type IV (full converter) wind power conversion systems exclusively.

SI proposals can be divided into two categories: open loop and closed loop. Open loop approaches are based on detecting a frequency event for which a pre-defined kinetic energy release is performed [2]. Closed loop proposals develop SI feedback controllers that measure system state variables to release kinetic energy depending on the magnitude of the event, emulating the functioning of synchronous generator governors. Closed-loop strategies have shown better performance, proposing, in general, a gain that decreases with wind speed under various criteria for maintaining stability [3].

Detailed revisions of current SI techniques can be found in [4]–[7]. In the literature, various definitions of SI can be found, see, for example, [8], [9]. However, most definitions relate SI only with a proportional response to the Rate of Change of Frequency (RoCoF). In our case, SI will refer to withdrawing kinetic energy from the moving part of the turbine in response to a frequency change, considering RoCoF and other state variables that participate in the dynamic phenomenon.

Among current closed-loop SI approaches, no particular attention is paid to controller parameter choice to maximize performance. These approaches basically propose a control law that represents the dynamic limitations on the amount

The associate editor coordinating the review of this manuscript and approving it for publication was Guangya Yang.

of kinetic energy that can be stably withdrawn from the VSWT; for example, [10] proposes an energy constraint to a linear controller to account for the dynamic limitations with a stabilising low-pass filter. Similarly, in [11], a simplified constraint representing the feasible choice of a SI linear controller is added to an economic operation formulation. In general, theses approaches are simple, and consider frequency as the only feedback variable; however, they cannot ensure an optimal behavior of the entire dynamic phenomena as they are focused on maintaining stability, overlooking performance optimization. Similar approaches are found in [12]–[14].

More detailed proposals concerning parameter tuning consider more advanced control techniques. In [15], a linearization of a VSWT and a power system are merged together into one equivalent dynamic system to define an operating security region, where system frequency deviation is represented. The region is such that a maximum frequency deviation is allowed, so a performance constraint is formulated; the work proposes an algorithm to obtain the security region. In [16], the algorithm in [15] is optimized. Also, a supervisory control strategy is proposed for the trajectory of the equivalent dynamic system to remain inside the security region, with a proportional control strategy on the derivative of the Center of Inertia (CoI) frequency. The controller commutates to an active mode while inside the security region and becomes off-line while outside of it. In terms of stability, the proposal in [16] considers a definition of the control gain in [2] that assumes a minimum VSWT speed of 0.7 p.u as an assessment of stability, which, presumably, prevents the linear equivalent from excessive deviations from the actual nonlinear dynamics. In terms of performance, the study proposes a method to decide when to switch on and off the control action; however, the control action when the controller is in switched on mode also depends on the control gain that follows the definition in [2]. The choice of the gain does not follow a performance-maximizing criterion.

Other recent works have considered an explicit definition of performance by the use of optimal control indexing; in particular, the H_∞ and H_2 norms. Conceptually, the H_∞ approach minimizes the effect of the worse case disturbance [17]. The H_2 control frameworks seek to minimize the energy of an output performance signal when affected by impulse disturbance, making the impact of the control strategy on minimizing a particular state variable easier to interpret [17].

In the context of SI control approaches, [18] considers a one-bus dynamic equivalent of a power systems to formulate a H_∞-based controller. The H_∞ controller is focused on minimizing the value of the largest spectral component of system frequency. The controller is assumed to be centralized and operates on one single VSWT, which poses various concerns on the applicability on real power systems where various wind turbines are grouped in one wind plant that are normally distributed over extensive geographical areas. Similarly, it is difficult to assess the impact of the H_∞ control proposal on specific frequency adequacy metrics such as the RoCoF or Nadir (the lowest point of the frequency transient) as the H_∞ controller is focused on minimizing the value of the largest spectral component of the norm of the state vector. The work in [19] also considers a H_∞-based controller in comparison to a Linear Quadratic Regulator (LQR) controller. The proposal also formulate a one-bus approximation and one controller, presenting the same limitations as [18] in terms of overlooking multi-wind turbine operation. The LQR example in [19] uses some elements of H_2 control, but a definition of a specific frequency control performance metric is not considered. The results above have the limitations of overlooking a multi-wind turbine scenario and an explicitly representation of a frequency control performance metrics as RoCoF or Nadir. To the best knowledge of the authors, no previous research has been focused on the multi-wind turbine stability problem and on explicitly representing frequency control performance metrics as RoCoF or Nadir.

This paper proposes a SI control strategy to both minimize frequency RoCoF and ensure stable multi-wind turbine operation considering an H_2 norm control technique. First, the H_2 formulation will allow an explicit definition of frequency control performance, which in this case will be focused on system RoCoF, allowing a better representation of the actual role of inertia in Power Systems. Second, a stability proof is presented, where the definition of distributed controllers associated with different VSWTs operating under different wind speeds is represented. To obtain numerical results, a reduced-order, empirically-validated model of the Electric Reliability Council of Texas (ERCOT) is considered. The points above cannot be found in the literature under the concept of either synthetic inertia or Fast Frequency Response.

Notation: I_n is the $n \times n$ identity matrix, 0_n and $0_{m\times n}$ are the $n \times n$ and $m \times n$ matrices of zeros, respectively. For a real matrix M, M^T denotes its transpose, and $M > 0 (< 0)$ means that M is symmetric and positive-definite (negative-defined). $det\{M\}$ stands for the determinant of M and $Diag\{M_1, \ldots, M_n\}$ is the block diagonal matrix with M_i matrices lying along the diagonal.

II. POWER SYSTEM FREQUENCY DYNAMICS MODEL

As commonly seen in SI studies [18], [19], this work will consider a dynamic equivalent of system frequency, particularly the model presented in [20]. This model is focused on frequency stability, and simplifies the representation of other dynamic phenomena in order to facilitates the frequency stability analysis. A detailed description and validation of this model can be also found in [21], and its block diagram representation can be seen in Fig. 1. Using synchrophasor data of generation contingencies, a predictive error identification process [22] is used to obtain the model parameters representing an actual frequency behavior in the case of Texan interconnection (ERCOT).

The model, that has been used to represent the frequency dynamics of the ERCOT [20], Nordic [23] and Chilean [24] power systems, can be modified to represent the response of SI control strategies. Moreover, the damping coefficient of

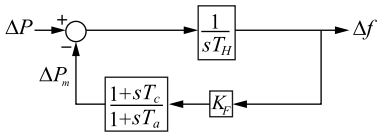

FIGURE 1. Simplified model of frequency dynamics [20].

the frequency dynamics will be neglected as a simplifying assumption [25].

The model has been modified to include a power input from a SI control strategy by adding a new term in the sum point, that represents the additional power that comes from the wind energy system, namely ΔP_ω. The state-space representation of the simplified model is shown in (1).

$$\dot{X}_s = A_s X_s + B_s \Delta P_\omega + B_{sw} \Delta P \tag{1}$$

where,

$$X_s = \begin{bmatrix} \Delta f \\ \Delta P_m \end{bmatrix}, \quad A_s = \begin{bmatrix} 0 & \frac{-1}{T_H} \\ \frac{K_f}{T_a} & \frac{-K_f}{T_a}\left(1 + \frac{T_c}{T_H}\right) \end{bmatrix},$$

$$B_s = B_{sw} = \begin{bmatrix} \frac{1}{T_H} \\ \frac{K_f T_c}{T_a T_H} \end{bmatrix},$$

Δf : system frequency deviation (Hz),
ΔP_m : system governors power response (MW),
ΔP : system power balance (MW),
T_H : system inertia (s),
ΔP_ω : SI delivered power (MW),
T_a, T_c : model dynamic parameter (s), and
K_f : governor droop of the system (MW/Hz).

As detailed in [20], the parameters T_a, T_c, K_f, and T_H are identified to represent an actual data; in this case, data of a low load condition in the ERCOT system in January 26th, 2010 at 1:58am is identified. This condition represents a scenario of low inertia, with low load and low number of synchronous machines online. The identified parameters are shown in Table 1 and the identified frequency response in Fig. 2

TABLE 1. Identified parameters [20].

Load (MW)	Wind (MW)	Loss (MW)	T_H $(\frac{MW}{sHz})$	T_a (s)	T_c (s)	K_H $(\frac{MW}{Hz})$
27280	2360	798	6130	3.95	1.21	5207

The model in (1) represents the CoI (Center of Inertia), as it is usually in advanced control SI studies [18], [19].

III. WIND POWER PLANT MODEL AND SI CONTROL

The one-mass VSWT model proposed in [26] is adapted to represent SI control and the dynamics of a wind turbine as

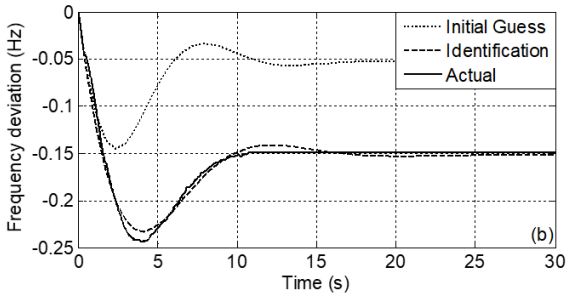

FIGURE 2. Identified dynamic behavior [20].

shown below:

$$\begin{aligned}
\dot{\omega}_r &= \frac{1}{J_w} T_m - \frac{1}{J_w} T_e - \frac{N_{gb}}{J_w} T_{SI}, \\
\dot{T}_e &= N_{gb}\left(k_p \dot{\omega}_r + k_i[\omega_r - \omega_{ro}(v_\omega)]\right), \\
P_w &= N_{gb} T_e \omega_r, \\
\Delta P_w &= N_{gb} T_{SI} \omega_r, ta), \\
T_m &= \frac{P_{wind}}{\omega_r} = \frac{0.5\rho A v_w^3 C_P(\lambda, \beta)}{\omega_r}, \\
C_P(\lambda, \beta) &= 0.645\{0.00912\lambda + \frac{-5 - 0.4(2.5+\beta) + 116\lambda_i}{e^{21\lambda_i}}\}, \\
\lambda_i &= \frac{1}{\lambda + 0.08(2.5+\beta)} - \frac{0.035}{1 + (2.5+\beta)^3},
\end{aligned} \tag{2}$$

where

ω_r : VSWT mechanical speed (rad/s),
J_w : VSWT moment of inertia (Kg· m^2),
T_m : VSWT mechanical torque (MNm),
T_e : torque reference from the Maximum Power Point Tracking (MPPT) control (MNm),
T_{SI} : torque reference from the SI control (MNm).
N_{gb} : gearbox conversion factor,
k_p, k_i : proportional and integral gains of MPPT control,
ω_{ro} : Tip Speed Ratio (TSR) reference (rad/s),
v_ω : wind speed (m/s),
ρ : air density (kg/m^3),
A : rotor-swept area of a VSWT (m^2),
P_{wind} : VSWT power input from wind (MW),
P_w : VSWT power output (MW),
ΔP_w : VSWT SI power output (MW),
λ : VSWT tip speed ratio,
β : VSWT pitch angle.

Note that ω_{ro} is the speed leading to the optimal TSR condition (maximum energy generation) for a particular wind speed v_ω, for which there also exists an optimal TSR torque $T_{\omega o}$. For control purposes, consider a linearization of system (2) for a set n of wind turbines with $i = 1, .., n$:

$$\begin{aligned}
\dot{\bar{X}}_i &= \bar{A}_i \bar{X}_i + \bar{B}_i \Delta T_{(SI)i}, \\
\Delta P_{wi} &= \bar{C}_i \bar{X}_i + \bar{D}_i \Delta T_{(SI)i},
\end{aligned} \tag{3}$$

where $\bar{X}_i = [\Delta\omega_{ri}\ \Delta T_{ei}]^T$, $\Delta\omega_{ri} \in R$ and $\Delta T_{ei} \in R$ are the wind speed deviation and electrical torque deviation from the

VSWT operation point, respectively. Moreover, $\bar{A}_i \in R^{2\times 2}$, $\bar{B}_i \in R^{2\times 1}$, $\bar{C}_i \in R^{1\times 2}$ and $\bar{D}_i \in R$ are numerical matrices obtained from the linearization process.

As seen in the literature, SI controllers measure system state variables and act on the turbine through $\Delta T_{\mathrm{SI}i}$, coupling systems (1) and (3). In particular, one can define a constant feedback state control strategy that measures the state variables to deliver a control action $T_{\mathrm{SI}i}$ for a particular wind turbine i, as shown in Fig. 3.

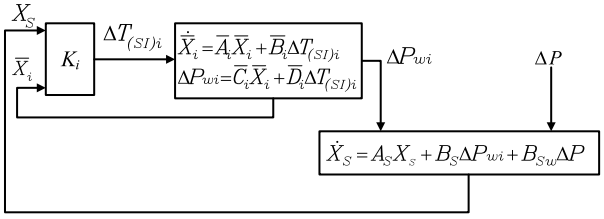

FIGURE 3. Dynamic interactions between a power system and a particular wind turbine *i*.

Note that the resulting 1-wind turbine system has now four state variables: Δf, ΔP_m, $\Delta\omega_{ri}$, ΔT_{ei}, which are the connection of the states space variables X_S of (1) and $\bar{X}_i$ of (3).

Assuming $K_i = [k_{i1}\ k_{i2}\ k_{i3}\ k_{i4}]$ as control gain, the state feedback control law is given by $T_{(SI)i} = K_i\varsigma$. The current advanced SI control techniques aim to compute a particular gain K_i in order to maximize the contribution of the SI control strategy to system frequency stability for the one- VSWT case. With the above consideration, the one wind turbine, closed-loop system is given as follows:

$$\dot{\varsigma} = (A_i + B_{ui}K_i)\varsigma + B_w w, \tag{4}$$

where,

$$\varsigma = \begin{bmatrix} X_s \\ \bar{X}_i \end{bmatrix}, \quad A_i = \begin{bmatrix} A_s & B_s\bar{C}_i \\ 0 & \bar{A}_i \end{bmatrix},$$
$$B_{ui} = \begin{bmatrix} B_s\bar{D}_i \\ \bar{B}_i \end{bmatrix}, \quad B_w = \begin{bmatrix} B_{sw} \\ 0 \end{bmatrix}$$

where $\varsigma \in R^{4\times 1}$ is the state vector, $A_i \in R^{4\times 4}$, $B_{ui} \in R^{4\times 1}$ and $B_w \in R^{4\times 1}$ are constant matrices representing the coupled linearized dynamic system with $w = \Delta P \in R$.

IV. OPTIMAL SI CONTROLLER

In this section, a RoCoF-minimizing approach is presented.

A. BASIC IDEA

Most advance control proposals of SI in the state of the art use the H_∞ norm to represent performance of the SI control action. The H_∞ norm primarily concerns with the peaks in the frequency spectrum in response to a energy-bounded disturbance, which is normally associated with a sudden power balance change. This way, the impact of the H_∞ norm on direct frequency adequacy metrics, such as RoCoF or Nadir, is not easy to assess. The H_∞ proposals in the literature show some effect on arresting RoCoF or Nadir, but the objective function given by minimizing the H_∞ norm of the state vector is not explicitly related to RoCoF or Nadir.

Also, the general concept of inertia is more related with the RoCoF. The inertia of a synchronous machine is associated with the kinetic energy that is released to maintaining power system balance, and it is, mathematically, inversely proportional to the RoCoF the first instants of a frequency transient after a sudden loss of power balance [27]. Therefore, the SI concept in an advance control framework should be explicitly associated to RoCoF to better emulate the actual physical meaning of inertia in a power system.

In this context, the H_2 control theory better suits the conditions given above. The H_2 control theory minimizes state variable energy in response to an impulse disturbance. If one can define the objective function of the H_2 control to minimize the energy of RoCoF, the control proposal will better represent the fundamentals of inertia and the core aim of the control action. However, this idea has two main complexities:

- RoCoF is not a state variable of dynamic model (4), and
- the H_2 theory requires the perturbation signal to be an impulse, while the perturbation to the SI controller is a step function (a sudden loss of power balance).

The following sections develop a model to allow a H_2 formulation to minimize the RoCoF in a SI proposal.

B. MINIMIZATION OF H_2 AND RoCoF

Note that the disturbance ΔP can be mathematically described as a step function, making it challenging to employ the H_2 approach. However, if ΔP is a step function, then $\Delta\dot{P}$ is an impulse function that can fulfill the conditions for the H_2 control. In order to take advantage of this fact, consider a new system that is obtained from the time derivative of (4), by defining $\varepsilon = \dot{\varsigma}$

$$\begin{aligned} \dot{\varepsilon} &= (A_i + B_{ui}K_i)\varepsilon + B_w\bar{w}, \\ z &= (C + DK_i)\varepsilon, \end{aligned} \tag{5}$$

where $\bar{w} = \dot{w}$ is an impulse signal. The matrices A_i, B_{ui} and B_w are given in (4), and z is the output performance signal, where the matrices C and D are selected in function of the performance goal. Note that the system (5) contains the derivatives of the original state vector, so defining $C = [1\ 0\ 0\ 0]$ and $D = 0$, the output performance signal z is the derivative of the frequency, that is, $z = \Delta\dot{f}$ = RoCoF. Because of that, the transference matrix function $G(\cdot)$, between $\bar{w}$ and z for system (5) represents the relation between the impulse signal $\Delta\dot{P}$ and the RoCoF energy, which is the energy of the frequency RoCoF. Thus, from the H_2 control approach theory, it is possible to design a control gain K_i in order to minimize the RoCoF energy while guaranteeing stability for system (5). for a given gain matrix K_i, the H_2-norm for the $G(\cdot)$ is given by:

$$\|G(\cdot)\|_2^2 = \mathrm{trace}\{(C + DK_i)\bar{P}(C + DK_i)^T)\}, \tag{6}$$

where $\bar{P}$ is the solution of the following Riccati Equation: $(A_i + B_{ui}K_i)\bar{P} + \bar{P}(A_i + B_{ui}K_i)^T + B_wB_w^T = 0$.

Alternatively, in order to design a gain matrix K_i that minimize the H_2-norm of the $G(\cdot)$ for one turbine system i, the following computable approach based on Linear Matrix Inequalities (LMI) can be formulated [28]:

$$\begin{aligned} &\min_{Z=Z^T, P=P^T, W} \quad trace\{Z\} \\ &s.a. \\ &\quad A_iP + B_{ui}W + (A_iP + B_{ui}W)^T + B_wB_w^T < 0, \\ &\quad \begin{bmatrix} Z & CP + DW \\ (CP + DW)^T & P \end{bmatrix} > 0. \end{aligned} \tag{7}$$

Thus, when the above optimization problem has a solution, the feedback control gain $K_i = WP^{-1}$ ensures that the system (5) is stable and also that $\|G(\cdot)\|_2^2 \leq trace\{Z\}$, which means that the RoCoF energy is minimized.

Since the system is linear and all system matrices are time-invariant, if there exists a matrix K_i such that system (5) is stable and minimizes the RoCoF energy, the same gain matrix K_i ensures also that (4) is stable with a minimized RoCoF energy. Moreover, since $\varepsilon = \dot{\varsigma}$, then the control law for system (5) is given by $\dot{u} = \dot{T}_{(SI)i} = K_i\varepsilon$. Applying the time integral operator in all terms in the last equation, one obtains that the control law for the system (4), which ensures system stability and minimized RoCoF energy, is given by

$$u = T_{(SI)i} = K_i\varsigma, \tag{8}$$

C. LIMITATIONS OF THE LINEARIZATION

To apply the method described in Section IV-B, the system (2) must be linearized. In general, the various proposals on SI consider linear equivalents of system (2), claiming that the linear representation is sufficient to represent the underlying nonlinear phenomenon [18], [19]. However, in the case presented, if one computes the gain K_i using the method in Section IV-B and then implements the proportional controller in the nonlinear system (2), the control action may fail in maintaining stability because of the lack of representativeness of the linear equivalent, as shown in the scheme in Fig. 4.

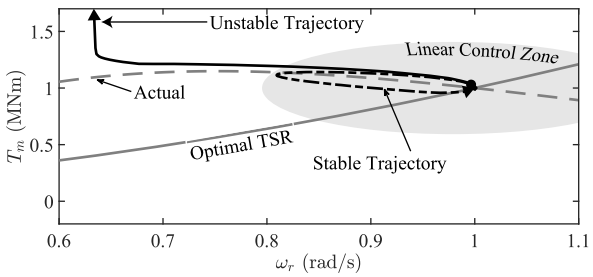

FIGURE 4. Impact of the nonlinearity on the closed-loop system stability under the control policy proposed in Section IV-B $V_W = 11$ m/s.

In Fig. 4, one can see that the torque-speed relationship of the VSWT presents a nonlinear region around the maximum torque point. If the control action drives the system towards that region, stability is compromised. Most SI approaches prevent turbine speed from dropping below 0.7 p.u. [2] as an *ad-hoc* limit.

In order to avoid fixed limits for VSWT speed, this work reformulates the H_2 control problem to prevent the control action from driving the system into the nonlinear region.

D. AN LQR APPROACH TO ADDRESS THE LINEAR MODEL REPRESENTATIVENESS

From the optimal control theory, a Linear Quadratic Regular (LQR) control approach can be considered [29]. The LQR control aims to compute a feedback proportional control gain K for system (5) in order to minimize the quadratic cost functional J given by:

$$J = \int_0^\infty (\epsilon^T Q x + u^T R u)\, dt, \tag{9}$$

where the matrices Q and R are symmetric positive definite matrices which represents the weights, respectively, of the state variables and the control efforts. The quadratic cost functional J represents the trade-off between the state rate convergence and the control effort.

Since Q and R are symmetric positive definite matrices, one can obtain their Cholesky factorization given by

$$Q = (Q^{\frac{1}{2}})^T Q^{\frac{1}{2}}, \quad R = (R^{\frac{1}{2}})^T R^{\frac{1}{2}}. \tag{10}$$

On the other hand, note that if in (5) one defines

$$C = \begin{bmatrix} Q^{\frac{1}{2}} \\ 0 \end{bmatrix}, \quad D = \begin{bmatrix} 0 \\ R^{\frac{1}{2}} \end{bmatrix}, \tag{11}$$

then $\|G(\cdot)\|_2^2$ in (6) is exactly described by the quadratic cost functional J in (9). This way, LQR can be seen as a particular case of the H_2 norm when the matrices C and D are given by (11). Then, considering (11) in (7), and applying the Schur complement (see more details in [30]), the optimization problem in (7) can be rewritten as:

$$\begin{aligned} &\min_{Y=Y^T, P=P^T, W} \quad \gamma \\ &s.t. \\ &\quad A_iP + B_{ui}W + (A_iP + B_{ui}W)^T + B_wB_w^T < 0 \\ &\quad trace\left(Q^{\frac{1}{2}} X (Q^{\frac{1}{2}})^T\right) + trace(Y) < \gamma \\ &\quad \begin{bmatrix} Y & R^{\frac{1}{2}}W \\ (R^{\frac{1}{2}}W)^T & P \end{bmatrix} > 0. \end{aligned} \tag{12}$$

where γ is a scalar and the feedback control gain is given by $K = WP^{-1}$.

In this scenario, Q and R are matrices that must be selected. In this work, these matrices will play an important role in the representativeness of RoCoF and in the stability of the linear controller on the nonlinear system (2).

1) DETERMINATION OF Q

In order to ensure that the performance output signal represents the RoCoF, it is necessary to select adequately the weighting matrix Q, which represents the states energy.

In system (5), the first component of the state vector is the derivative of frequency, so one can define the following Q matrix:

$$Q = \begin{bmatrix} \beta & 0 & 0 & 0 \\ 0 & \delta & 0 & 0 \\ 0 & 0 & \delta & 0 \\ 0 & 0 & 0 & \delta \end{bmatrix} \tag{13}$$

where δ and β are positive numbers, and $\delta \ll \beta$. Since $\delta \ll \beta$ and $\varepsilon = [\Delta\dot{f} \ \Delta\dot{P}_m \ \Delta\dot{\omega}_{ri}\Delta\dot{T}_{ei}]^T$, the performance index becomes $z \approx \Delta\dot{f}$, representing the RoCoF energy and mimicking the role of traditional inertia in frequency dynamics.

2) DETERMINATION OF R

Note that R represents a weight on the control action in the objective function of (9). Intuitively, a "large" R will limit the control action, reducing the impact of the control on reducing system RoCoF; a "small" R, conversely, will increase the impact of the control on reducing system RoCoF. However, a "small" R can drive the system to a region where the linear representation of (2) deviates from the actual system; this situation is depicted in Fig. 4.

As to increase the performance of the control on reducing system RoCoF, one can select the smallest R (namely R^*) so that the control action does not drive the state vector far from its linear behavior. Stability can be verified by simulation, and a specific criterion to determine the value of R^* can be established. The method is described in Fig. 5.

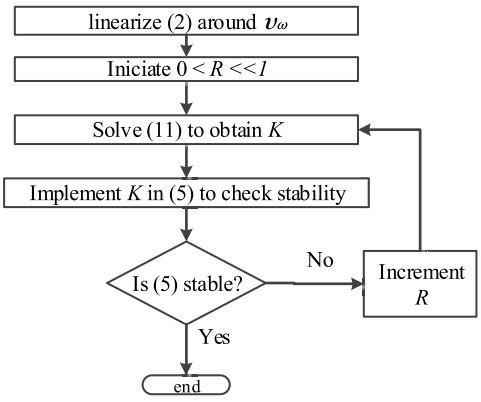

FIGURE 5. Algorithm for computing K and R for all admissible values of N_L and υ_ω to avoid instability.

Note that in every iteration of the algorithm a computation of the H_2 optimal control gains is obtained, so, together R^*, the corresponding K is obtained for that particular value of R^*.

E. DISTRIBUTED CONTROL STRATEGY

In recent works that use advanced control techniques for SI, the proposals consider one wind turbine connected to a power system, overlooking formal proof for cases with various wind turbines. For example, [31], [32] consider a technique that is defined for a one-wind turbine extrapolated to a multiple wind turbine case by simulation using participation factors. The simulations show a good performance of the multiple-wind turbine case, but no formal stability proof is provided. The following theorem guarantees the stable operation of multi-wind turbine SI systems.

Theorem 1: Consider the multi-turbine case with n wind turbines. It is assumed that each VSWT i, ($i = 1, .., n$) is described by system (3) *and is connected to the power system* (1) *as shown in Fig. 6. If for each turbine i there exists a control gain K_i for which the one turbine case (see Fig.* (3)*) is closed-loop stable, then the multi-turbine system represented in Fig. 6 is also stable.*

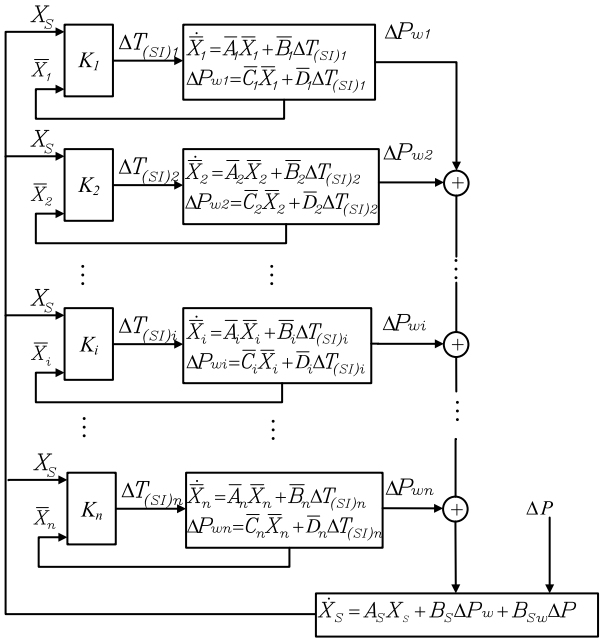

FIGURE 6. Dynamic relationships between a power system and a group of n wind turbines implemented with closed-loop SI.

Proof: The proof of this theorem can be found in the Appendix VII-A.

This allows the integration of SI controllers in a distributed manner, without considering re-tuning the existing controllers any time a new wind turbine is added with the proposed SI control or a wind turbine becomes offline due to the absence of wind. This result is similar to the way governor proportional controllers can be added/removed to/from a power system without stability concerns [21].

V. STUDY CASE

To show the applicability of the proposed SI control procedure, turbine the case of one and multi-wind turbines will be considered, as it is shown in Fig. 7. The simulations will consider that voltage, transient, and small signal stability issues are addressed, so voltage collapse, angle stability and power oscillations are controlled, as normally assumed in

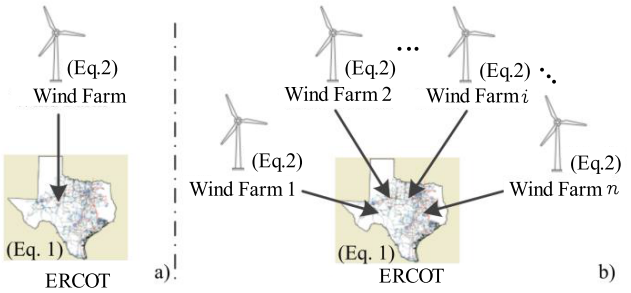

FIGURE 7. Simulation scenarios: a) one wind turbine, and b) Multi-wind turbine.

these analyses [18], [19]. This way, a one bus representation of the power system can be considered.

In all cases, three scenarios are considered: a base case with no SI control, a proportional to the frequency derivative, kinetic energy-based SI control from [33] (namely "KE control"), and the proposed case with the SI H_2 optimal control. It is important to note that the simulations consider the linear controller implemented in the nonlinear version of the VSWT dynamics.

To consider a realistic power system, the ERCOT empirically validated model shown in Section II is used; the ERCOT case is presented in detail in [20], where the parameters are tuned with empirical data as shown in Section II.

The wind turbine model (2) considers the parameters of a National Renewable Energy Laboratory (NREL) 5 MW Baseline VSWT model [34]. The parameters are shown in the annexes.

A. ONE WIND TURBINE CASE

A first simulation consists of a one-wind turbine case. Wind generation is modelled by 472 identical 5MW VSWTs, with an input wind speed of 11 m/s. This way, each turbine power output is 5 MW, accounting for a pre-fault aggregated power output of 2360 MW (to maintain the condition in Table 1). For the operating point ($v_\omega = 11$ m/s), one can obtain the linearization of the system described in Section III, and the controller parameters as explained in Section IV. The resulting controller parameters are $k_1 = -0.2484$, $k_2 = 1.5 \cdot 10^{-4}$, $k_3 = 0.70058$, $k_4 = 0.003316$, and $R = 0.46$. Then, a 798 MW sudden loss of generation is simulated in Fig. 8, 9 and 10, where the frequency, turbine speed, and SI power responses are shown respectively.

It can be seen in Fig. 8 that RoCoF significantly decrease with respect to the base case, showing the action of the SI control. The proposed technique is also better than the KE SI in terms of RoCoF. The improved RoCoF response has also a positive impact on the Nadir; although the control effort is only constrained to minimize RoCoF, the slower frequency behavior helps the governor response to reduce the Nadir.

The VSWT speed is shown in Fig. 9. In the case of the KE control, turbine speed decreased by about 2%, while the H_2 control allows a minimum turbine speed of about 5%.

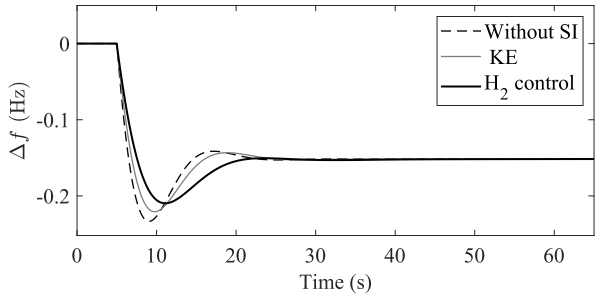

FIGURE 8. Frequency response for the 1-wind turbine case: Without SI control, KE control proposed in [33], and the proposed H_2 control method.

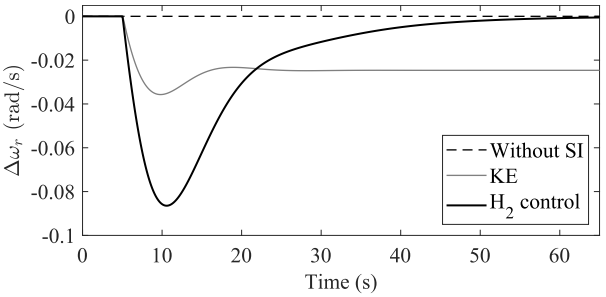

FIGURE 9. Turbine speed response for the 1-wind turbine case: Without SI control, KE control proposed in [33], and the proposed H_2 control method.

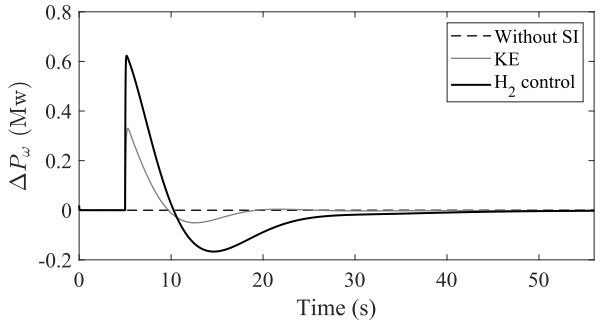

FIGURE 10. Turbine power response for the 1-wind turbine case: Without SI control, KE control proposed in [33], and the proposed H_2 control method.

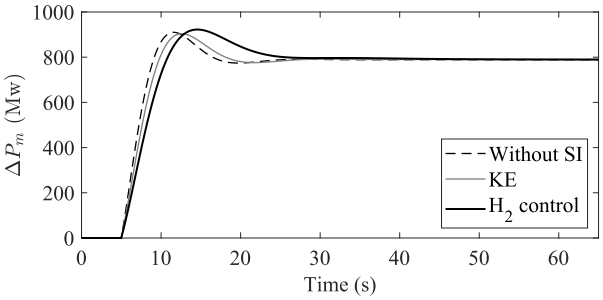

FIGURE 11. Turbine power response for the 1-wind turbine case.

The largest allowance in the case of the H_2 control is given by the more detailed representation of the stability limit ensured by the algorithm in Fig. 5. Also, and in order to restore turbine speed to the pre-fault MPPT operating value, the H_2 control

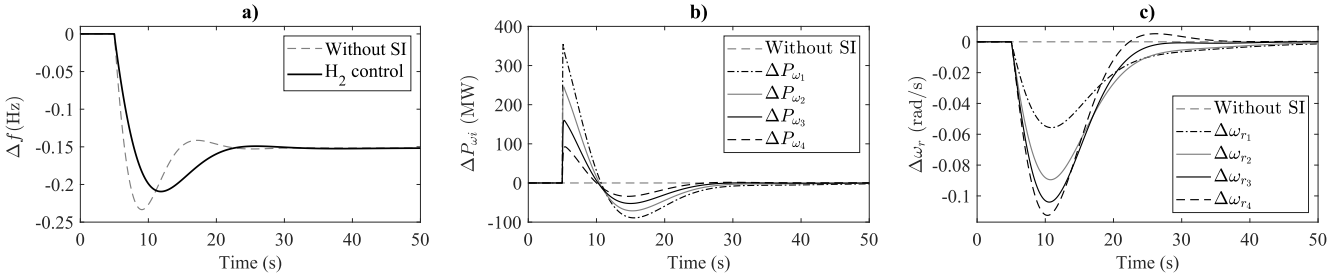

FIGURE 12. Results for the 4-wind turbine case. Figures b) and c) show incremental values from P_0 and ω_{ro} in Table 2.

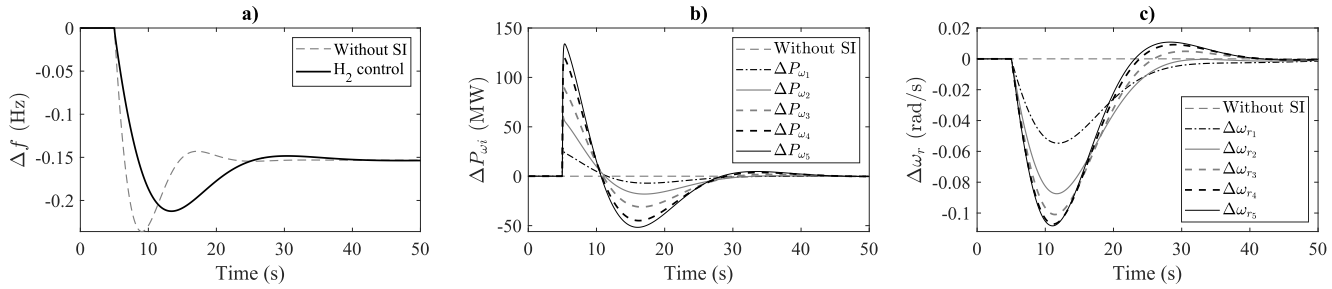

FIGURE 13. Results for the 5-wind turbine case. Figures b) and c) show incremental values from P_0 and ω_{ro} in Table.

accelerates the turbine, which shows the integration of the normal MPPT controller to the H_2 controller. In the case of the KE control, the formulation is not designed include the MPPT controller, so the turbine speed is not recovered to pre-fault values and reaches a steady state value with a significant offset.

The VSWT SI power contribution is shown in Fig. 10. The power contribution of the H_2 control is larger in peak and duration than that of the KE control; however, the H_2 control presents a large recovery period in which power is withdrawn from the grid (starting about 10s in Fig. 10). This power withdrawal is necessary for the turbine to accelerate to its pre-fault MPPT operating point, as seen in Fig. 9. As the KE control does not represent the MPPT controller, the lost of the pre-fault MPPT operating point is not addressed.

The overall governor response is shown in Fig. 11. It can be seen that the reduced RoCoF allows governors to respond with a slower ramp rate, reducing the need for faster synchronous generation. Various power system operators are implementing fast frequency response ancillary service products; a reduction on required ramprates also contributes to reduce the required ancillary services and costs of renewable integration.

B. MULTI-WIND TURBINE CASE

A second case considers 4 and 5 wind turbine simulations with different wind speeds. In this case it was not possible to simulate the KE control, since the KE control proposal was not designed for a multi-wind turbine scenario. In four-wind turbine and five-wind turbine simulation each group of wind

TABLE 2. Simulation parameters for the 4-wind turbine case.

i	Units of Turbines	v_ω (m/s)	ω_{ro} (rad/s)	P_0 (MW)	R
1	296	4	0.629	71	0.97
2	296	6	0.943	240	0.50
3	296	8	1.257	569	0.47
4	296	11	1.729	1480	0.46

TABLE 3. Simulation parameters for the 5-wind turbine case.

i	Units of Turbines	v_ω (m/s)	ω_{ro} (rad/s)	P_0 (MW)	R
1	201	4	0.629	48	0.97
2	201	6	0.943	163	0.50
3	201	8	1.257	388	0.47
5	201	10	1.572	756	0.47
4	201	11	1.729	1005	0.46

turbine consists of 296 and 201 turbines units, respectively, for which the pre-fault overall wind power output accounts for 2360 MW (maintaining the condition in Table 1). The simulation parameters are shown in Table 2 and Table 3. The H_2 control parameters are shown in the Appendix.

Fig. 12 and Fig. 13 shows the response of the system for a 798 MW contingency. In terms of the power response, a larger wind speed corresponds with a larger power response. In terms of VSWT speed, all cases behave similarly; the largest operating points correspond with larger speed drops, which are associated with smaller values of R (a less restrictive control action). The torque-speed relationship for larger wind speed values has a larger region in which the linear

representation is closer to the nonlinear system; this is consistent with the values of R in Table 2 and 3. Overall, the operation for a distributed control scenario and different wind speed for the controllers is shown to be stable.

VI. CONCLUSION

This work proposes the H_2 optimal control method as a SI control strategy. First, a mathematical proof of multi-wind turbine stability has been proposed in Theorem 1, which ensures complete close loop stability for the multi-wind turbine case. Note that this is an important result since most current approaches only ensure close loop stability for the multi-wind turbine by simulation. Second, a new SI control strategy is proposed. The proposed control strategy has the advantage of representing RoCoF directly as a control performance metric using the H_2 control properties to minimize the RoCoF energy, while current methods are based on H_∞ with less clear connection to RoCoF minimization specifically. In addition, an LQR approach was proposed to deal with the nonlinearity of the real model, allowing the controller to work on the nonlinear model. Numerical results considering 1, 4, and 5 wind turbine scenarios are presented, showing the improved performance of the method in minimizing the RoCoF and its validity concerning multi-wind turbine cases.

The effect of external disturbances, such as power imbalances are explicitly considered in the proposed SI control design. However, internal disturbance are not considered. They can be originated by various phenomena, such as changes in wind speed leading to different parameters for the linearized system or changes in power system scheduling leading to changes in the parameters describing the underlying dynamics of the power system. Future work will focus on extending the minimal RoCoF control design and multi-turbine stability to the case of systems affected by internal disturbances. Particular attention will be given to modeling and designing the H_2 control to ensure robustness under internal disturbance.

In addition, wind turbine manufacturers usually set hard limits on how much and how fast energy can be released, and how fast the energy can be restored. These limitations are associated with power electronics ratings, mechanical acceleration limitations, etc. Future work will consider an integration of these limitations into the control algorithms.

VII. APPENDIX

A. PROOF OF THEOREM 1

Before presenting the proof of the Theorem 1, some previous results about Matrix Analysis are cited. For more information about this subject, one can see [35] and references therein.

1) FACTS ON BLOCK MATRICES

Consider $\mathbb{A} \in R^{n\times n}$, $\mathbb{B} \in R^{n\times m}$, $\mathbb{C} \in R^{m\times n}$, $\mathbb{D} \in R^{m\times m}$, and that there exits $\mathbb{A}^{-1}$, then

$$det\left(\begin{bmatrix}\mathbb{A} & \mathbb{B}\\ \mathbb{C} & \mathbb{D}\end{bmatrix}\right) = det(\mathbb{A})det(\mathbb{D} - \mathbb{C}\,\mathbb{A}^{-1}\mathbb{B}). \quad (14)$$

Lemma 1: [30] *A matrix $\mathbb{A} \in R^{n\times n}$ has all its eigenvalues with real negative part if $\mathbb{A} + \mathbb{A}^T < 0$.*

Lemma 2: [36] *If $\mathbb{A} \in R^{n\times n}$ is an non-singular matrix, and $\mathbb{U}$ and $\mathbb{V}$ are $n \times m$ matrices, then*

$$det(\mathbb{A} + \mathbb{U}\mathbb{V}^T) = det(I_m + \mathbb{V}^T\mathbb{A}^{-1}\mathbb{U})det(\mathbb{A}).$$

Proof of Theorem 1: Note that, for each turbine i, the control law $T_{(SI)i} = K_i\varsigma$ can be divide as

$$T_{(SI)i} = K_{ai}X_s + K_{bi}\bar{X}_i, \quad (15)$$

where $X_s = [\Delta P_m \;\; \Delta f]$, $\bar{X}_i = [\Delta\omega_{ri} \;\; \Delta T_{ei}]$, as defined in Section III. Considering systems (1) and (3) for each i, $(i = 1, .., n)$, without considering the disturbance, the multi-turbine state-space equation for the dynamical system in Figure 6 is given by

$$\begin{bmatrix}\dot{X}_s\\ \dot{\bar{X}}_1\\ \dot{\bar{X}}_2\\ \vdots\\ \dot{\bar{X}}_n\end{bmatrix} = \underbrace{\begin{bmatrix}A_{cls} & B_s\bar{C}_{cl1} & B_s\bar{C}_{cl2} & \cdots & B_s\bar{C}_{cln}\\ \bar{B}_1K_{a1} & \bar{A}_{cl1} & 0 & \cdots & 0\\ \bar{B}_2K_{a2} & 0 & \bar{A}_{cl2} & \cdots & 0\\ \vdots & \vdots & \vdots & \ddots & 0\\ \bar{B}_nK_{an} & 0 & 0 & \ldots & \bar{A}_{cln}\end{bmatrix}}_{M}\begin{bmatrix}X_s\\ \bar{X}_1\\ \bar{X}_2\\ \vdots\\ \bar{X}_n\end{bmatrix} \quad (16)$$

where $A_{cls} = A_s + B_s\sum_{i=1}^{n}\bar{D}_iK_{ai}$, $\bar{A}_{cli} = \bar{A}_i + \bar{B}_iK_{bi}$ and $\bar{C}_{cli} = \bar{C}_i + \bar{D}_iK_{bi}$ By hypothesis, for each turbine i there exists a control gain K_i for which the individual closed-loop control system is stable (see Fig. (3)). Hence the subsystem (4), given by

$$\begin{bmatrix}\dot{X}_s\\ \dot{\bar{X}}_i\end{bmatrix} = \underbrace{\begin{bmatrix}A_s + B_s\bar{D}_iK_{ai} & B_s\bar{C}_{cli}\\ \bar{B}_iK_{ai} & \bar{A}_{cli}\end{bmatrix}}_{M_i}\begin{bmatrix}X_s\\ \bar{X}_i\end{bmatrix} \quad (17)$$

is stable, so that the eigenvalues $\sigma(M_i)$ have negative real parts. Then, $M_{mi} = M_i^T + M_i$ is negative definite ($M_{mi} < 0$) for each i, which implies that $-M_{mi}$ is positive definite. It is well known that $-M_{mi}$ is a positive definite matrix then the determinants of all leading principal minors of $-M_{mi}$ are positive. Thus, assuming that $\alpha_{A_si} = A_s + B_s\bar{D}_iK_{ai} + (A_s + +B_s\bar{D}_iK_{ai})^T$, for each turbine i it is true that:

$$\begin{aligned} det(-M_{mi}) > 0, \quad det(-\alpha_{A_{si}}) > 0,\\ det(-(\bar{A}_{cli} + \bar{A}_{cli}^T)) > 0 \end{aligned} \quad (18)$$

On the other hand, the stability of the multi-turbine case (16) depends on the eigenvalues $\sigma(M)$. By the Lemma 1, we have that the real part of the eigenvalues of M are negative if $M_m = M + M^T < 0$, or $-M_m$ is positive definite. Thus, it is necessary to show that the determinants of all leading principal minors of $-M_m$ are positive.

In other to show that $-M_m > 0$, note that M_m can be represented by the following block matrix:

$$M_m = \begin{bmatrix}A_{cls} + A_{cls}^T & \bar{\nu}_n^T\\ \bar{\nu}_n & D_{Acl_n}\end{bmatrix}.$$

where $\nu_i = \bar{B}_i K_{ai} + \bar{C}_{cli}^T B_s^T$,

$$\bar{\nu}_i^T = [\, \nu_1^T \quad \nu_2^T \quad \cdots \quad \nu_i^T \,], \quad \text{and}$$
$$D_{Acl_i} = Diag\{\bar{A}_{cl1} + \bar{A}_{cl1}^T, \bar{A}_{cl2} + \bar{A}_{cl2}^T, \cdots \bar{A}_{cli} + \bar{A}_{cli}^T\}.$$

Moreover consider that $\bar{M}_{m_{[j-1]}}$ is the j leading principal minor block of $-M_m$, for $j = 1, \ldots, n+1$, where

$$\bar{M}_{m_{[0]}} = -A_{cls} - A_{cls}^T,$$
$$\bar{M}_{m_{[i]}} = -\begin{bmatrix} A_{cls} + A_{cls}^T & \bar{\nu}_i^T \\ \bar{\nu}_i & D_{Acl_i} \end{bmatrix}, \quad \forall i = 1, \cdots, n$$

Using (14), the determinant of each leading principal minor block $\bar{M}_{m_{[j-1]}}, j = 1, \ldots, n+1$ of $-M_m$ is given by

$$det(\bar{M}_{m_{[0]}}) = det(-A_{cls} - A_{cls}^T)$$
$$det(\bar{M}_{m_{[i]}}) = det(-A_{cls} - A_{cls}^T) det(\,\Gamma_i\,), \quad \forall i = 1, \ldots, n \tag{19}$$

where $\Gamma_i = -D_{Acl_i} + \bar{\nu}_i \alpha_{A_s}^{-1} \bar{\nu}_i^T$.

As, for each turbine i, the closed loop system (17) is stable, and by (18), one can see that $det(-\alpha_{A_{si}}) > 0$ and $-D_{Acl_i} > 0$ for all i.

In order to show that $det(\bar{M}_{m_{[0]}})$ is always positive, note that

$$det(-A_{cls} - A_{cls}^T) = det(-\sum_{i=1}^{n} \alpha_{A_{si}} + \tilde{A}_s^{1/2} \tilde{A}_s^{1/2})$$

where $\tilde{A}_s = (n-1)(A_s + A_s^T)$.

By (18), one can see that the term $-\sum_{i=1}^{n} \alpha_{A_{si}}$ is non singular, since for each turbine i, $-\alpha_{A_{si}} > 0$. Thus, applying Lemma 2 we obtain that

$$det(-A_{cls} - A_{cls}^T) = det(\mathbb{A}_i) det(-\sum_{i=1}^{n} \alpha_{A_{si}})$$

where $\mathbb{A}_i = I_2 + \tilde{A}_s^{1/2} (-\sum_{i=1}^{n} \alpha_{A_{si}})^{-1} \tilde{A}_s^{1/2}$. Note that, since for each turbine, $-\alpha_{A_{si}}$ is positive defined matrix then $det(-\sum_{i=1}^{n} \alpha_{A_{si}}) > 0$ and $det(\mathbb{A}_i) > 0$, which implies that $det(\bar{M}_{m_{[0]}})$ is positive.

Now, in order to show that $det(\bar{M}_{m_{[i]}})$ is positive it is necessary to prove that $det(\,\Gamma_i\,)$ is always positive.

Note that, defining $\mathbb{V}_i = \bar{\nu}_i \alpha_{A_s}^{-1/2}$, we have that

$$det(\,\Gamma_i\,) = det(-D_{Acl_i} + \mathbb{V}_i \mathbb{V}_i^T). \tag{20}$$

The non-singularity of D_{Acl_i} allow us to apply Lemma 2 in (20), obtain that

$$det(\Gamma_i) = det(I_n + \mathbb{V}_i^T (-D_{Acl_i})^{-1} \mathbb{V}_i) det(-D_{Acl_i})$$

Since $-D_{Acl_i} > 0$, then $\mathbb{V}_i^T (-D_{Acl_i})^{-1} \mathbb{V}_i \geq 0$ which implies that $det(\Gamma_i) > 0$. Moreover this implies that the determinant of all leading principal minors in (19) of $-M_m$ are positive, that is $-M_m > 0$. The latter ensures that M_m is negative definite, proven by Lemma 1 that all eigenvalues of M are negative. Thus one can see that if each subsystem i is stable, then the global interconnect multi-turbine case in Figure 6 is also stable, which concludes the proof. □

B. NUMERICAL EXAMPLE MATRICES

1) SYSTEM

$$A_s = \begin{bmatrix} 0 & 1.6 \cdot 10^{-4} \\ -1.3 \cdot 10^3 & -0.51 \end{bmatrix},$$
$$B_s = \begin{bmatrix} -1.6 \cdot 10^{-4} \\ 0.26 \end{bmatrix},$$
$$B_{sw} = B_s \tag{21}$$

2) ONE WIND TURBINE CASE

$$\bar{A} = \begin{bmatrix} -0.15 & -11.27 \\ 0.17 & -1.63 \end{bmatrix}, \quad \bar{B} = \begin{bmatrix} -11.27 \\ -1.63 \end{bmatrix},$$
$$\bar{C} = \begin{bmatrix} 383.6 & 229.6 \end{bmatrix}, \quad \bar{D} = 229.6,$$
$$K = \begin{bmatrix} -0.2484 & 1.5 \cdot 10^{-4} & 0.70058 & 0.003316 \end{bmatrix} \tag{22}$$

3) MULTI-WIND TURBINE CASE

$$\bar{A}_1 = \begin{bmatrix} -0.0533 & -11.27 \\ 0.17 & -1.63 \end{bmatrix}, \quad \bar{B}_1 = \begin{bmatrix} -11.27 \\ -1.63 \end{bmatrix},$$
$$\bar{C}_1 = \begin{bmatrix} 50.73 & 83.479 \end{bmatrix}, \quad \bar{D}_1 = 83.479,$$
$$K_1 = \begin{bmatrix} -0.427 & 7.406 \cdot 10^{-5} & 1.844 & -0.002114 \end{bmatrix} \tag{23}$$
$$\bar{A}_2 = \begin{bmatrix} -0.08 & -11.27 \\ 0.17 & -1.63 \end{bmatrix}, \quad \bar{B}_2 = \begin{bmatrix} -11.27 \\ -1.63 \end{bmatrix},$$
$$\bar{C}_2 = \begin{bmatrix} 114.1 & 125.2 \end{bmatrix}, \quad \bar{D}_2 = 125.2,$$
$$K_2 = \begin{bmatrix} -0.469 & 1.1 \cdot 10^{-4} & 1.325 & -0.0766 \end{bmatrix} \tag{24}$$
$$\bar{A}_3 = \begin{bmatrix} -0.11 & -11.27 \\ 0.17 & -1.63 \end{bmatrix}, \quad \bar{B}_3 = \begin{bmatrix} -11.27 \\ -1.63 \end{bmatrix},$$
$$\bar{C}_3 = \begin{bmatrix} 202.9 & 166.9 \end{bmatrix}, \quad \bar{D}_3 = 166.9,$$
$$K_3 = \begin{bmatrix} -0.394 & 1.4 \cdot 10^{-3} & 1.038 & -0.01 \end{bmatrix} \tag{25}$$
$$\bar{A}_4 = \begin{bmatrix} -0.15 & -11.27 \\ 0.17 & -1.63 \end{bmatrix}, \quad \bar{B}_4 = \begin{bmatrix} -11.27 \\ -1.63 \end{bmatrix},$$
$$\bar{C}_4 = \begin{bmatrix} 383.6 & 229.6 \end{bmatrix}, \quad \bar{D}_4 = 229.6,$$
$$K_4 = \begin{bmatrix} -0.2484 & 1.5 \cdot 10^{-4} & 0.70058 & 3.3 \cdot 10^{-3} \end{bmatrix} \tag{26}$$
$$\bar{A}_5 = \begin{bmatrix} -0.13 & -11.27 \\ 0.17 & -1.63 \end{bmatrix}, \quad \bar{B}_5 = \begin{bmatrix} -11.27 \\ -1.63 \end{bmatrix},$$
$$\bar{C}_5 = \begin{bmatrix} 317.16 & 208.7 \end{bmatrix}, \quad \bar{D}_4 = 229.6,$$
$$K_5 = \begin{bmatrix} -0.2945 & 1.5 \cdot 10^{-4} & 0.798 & 4.8 \cdot 10^{-3} \end{bmatrix} \tag{27}$$

REFERENCES

[1] H. Kim, J. Lee, J. Lee, and G. Jang, "Novel coordinated control strategy of BESS and PMSG-WTG for fast frequency response," *Appl. Sci.*, vol. 11, no. 9, p. 3874, Apr. 2021. [Online]. Available: https://www.mdpi.com/2076-3417/11/9/3874

[2] S. Wang and K. Tomsovic, "A novel active power control framework for wind turbine generators to improve frequency response," *IEEE Trans. Power Syst.*, vol. 33, no. 6, pp. 6579–6589, Nov. 2018.

[3] J. Lee, G. Jang, E. Muljadi, F. Blaabjerg, Z. Chen, and Y. Cheol Kang, "Stable short-term frequency support using adaptive gains for a DFIG-based wind power plant," *IEEE Trans. Energy Convers.*, vol. 31, no. 3, pp. 1068–1079, Sep. 2016.

[4] Y. Cheng, R. Azizipanah-Abarghooee, S. Azizi, L. Ding, and V. Terzija, "Smart frequency control in low inertia energy systems based on frequency response techniques: A review," *Appl. Energy*, vol. 279, Dec. 2020, Art. no. 115798.
[5] T. Kerdphol, F. S. Rahman, M. Watanabe, and Y. Mitani, "An overview of virtual inertia and its control," in *Virtual Inertia Synthesis and Control* (Power Systems). Springer, Nov. 2020, pp. 1–11.
[6] A. Fernández-Guillamón, E. Gómez-Lázaro, E. Muljadi, and A. Molina-Garcia, "A review of virtual inertia techniques for renewable energy-based generators," in *Renewable Energy–Technologies and Applications*. Rijeka, Croatia: IntechOpen, Feb. 2021.
[7] V. Skiparev, R. Machlev, N. R. Chowdhury, Y. Levron, E. Petlenkov, and J. Belikov, "Virtual inertia control methods in islanded microgrids," *Energies*, vol. 14, no. 6, p. 1562, Mar. 2021.
[8] R. Eriksson, N. Modig, and K. Elkington, "Synthetic inertia versus fast frequency response: A definition," *IET Renew. Power Gener.*, vol. 12, no. 5, pp. 507–514, Apr. 2018.
[9] P. Fernández-Bustamante, O. Barambones, I. Calvo, C. Napole, and M. Derbeli, "Provision of frequency response from wind farms: A review," *Energies*, vol. 14, no. 20, p. 6689, Oct. 2021.
[10] M. Kosmecki, R. Rink, A. Wakszyńska, R. Ciavarella, M. Di Somma, C. N. Papadimitriou, V. Efthymiou, and G. Graditi, "A methodology for provision of frequency stability in operation planning of low inertia power systems," *Energies*, vol. 14, no. 3, p. 737, Jan. 2021.
[11] Z. Chu, U. Markovic, G. Hug, and F. Teng, "Towards optimal system scheduling with synthetic inertia provision from wind turbines," *IEEE Trans. Power Syst.*, vol. 35, no. 5, pp. 4056–4066, Sep. 2020.
[12] A. Mujcinagic, M. Kusljugic, and E. Nukic, "Wind inertial response based on the center of inertia frequency of a control area," *Energies*, vol. 13, no. 23, p. 6177, Nov. 2020.
[13] H. Gu, R. Yan, T. K. Saha, and E. Muljadi, "System strength and inertia constrained optimal generator dispatch under high renewable penetration," *IEEE Trans. Sustain. Energy*, vol. 11, no. 4, pp. 2392–2406, Oct. 2020, doi: 10.1109/tste.2019.2957568.
[14] F. Arredondo, P. Ledesma, E. D. Castronuovo, and M. Aghahassani, "Stability improvement of a transmission grid with high share of renewable energy using TSCOPF and inertia emulation," *IEEE Trans. Power Syst.*, early access, Sep. 7, 2020, doi: 10.1109/TPWRS.2020.3022082.
[15] Y. Zhang, K. Tomsovic, S. M. Djouadi, and H. Pulgar-Painemal, "Hybrid controller for wind turbine generators to ensure adequate frequency response in power networks," *IEEE J. Emerg. Sel. Topics Circuits Syst.*, vol. 7, no. 3, pp. 359–370, Sep. 2017.
[16] Y. Zhang, M. E. Raoufat, K. Tomsovic, and S. M. Djouadi, "Set theory-based safety supervisory control for wind turbines to ensure adequate frequency response," *IEEE Trans. Power Syst.*, vol. 34, no. 1, pp. 680–692, Jan. 2019.
[17] K. Zhou, J. Doyle, and K. Glover, *Robust and Optimal Control*. Upper Saddle River, NJ, USA: Prentice-Hall, 1996.
[18] D. M. Magnus, C. C. Scharlau, L. L. Pfitscher, G. C. Costa, and G. M. Silva, "A novel approach for robust control design of hidden synthetic inertia for variable speed wind turbines," *Electr. Power Syst. Res.*, vol. 196, Jul. 2021, Art. no. 107267.
[19] S. Morovati, Y. Zhang, S. M. Djouadi, K. Tomsovic, A. Wintenberg, and M. Olama, "Robust output feedback control design for inertia emulation by wind turbine generators," *IEEE Trans. Power Syst.*, vol. 36, no. 6, pp. 5056–5067, Nov. 2021.
[20] H. Chavez, R. Baldick, and S. Sharma, "Regulation adequacy analysis under high wind penetration scenarios in ERCOT nodal," *IEEE Trans. Sustain. Energy*, vol. 3, no. 4, pp. 743–750, Oct. 2012.
[21] P. Kundur, N. Balu, and M. Lauby, *Power System Stability and Control*. New York, NY, USA: McGraw-Hill, 1994.
[22] L. Ljung, "Convergence analysis of parametric identification methods," *IEEE Trans. Autom. Control*, vol. 23, no. 5, pp. 770–783, Oct. 1978.
[23] H. Chavez, M. R. Hezamsadeh, and F. Carlsson, "A simplified model for predicting primary control inadequacy for nonresponsive wind power," *IEEE Trans. Sustain. Energy*, vol. 7, no. 1, pp. 271–278, Jan. 2016.
[24] T. Avila, E. Gutierrez, and H. Chavez, "Perfomance standard-compliant secondary control: The case of Chile," *IEEE Latin Amer. Trans.*, vol. 15, no. 7, pp. 1257–1262, 2017.
[25] "Damping representation for power system stability studies," *IEEE Trans. Power Syst.*, vol. 14, no. 1, pp. 151–157, Feb. 1999.
[26] J. Roldán, "Simulación del funcionamiento de una turbina élica con generador de inducción doblemente alimentado," Ph.D. dissertation, Dept. de Ingeniería Eléctr., Universidad de Sevilla, Sep. 2015.
[27] *Inertia and Rate of Change of Frequency (RoCoF)*, European Network of Transmission System Operators for Electricity, Brussels, Belgium, 2020.
[28] S. Boyd, L. El Ghaoui, E. Feron, and V. Balakrishnan, *Linear Matrix Inequalities in System and Control Theory*. Philadelphia, PA, USA: SIAM, 1994.
[29] B. D. O. Anderson and J. B. Moore, *Optimal Control: Linear Quadratic Methods*. Upper Saddle River, NJ, USA: Prentice-Hall, 1990.
[30] G. Duan and H. Yu, *LMIs in Control Systems: Analysis, Design and Applications*. Boca Raton, FL, USA: CRC Press, 2013.
[31] J. Bjork, D. V. Pombo, and K. H. Johansson, "Variable-speed wind turbine control designed for coordinated fast frequency reserves," *IEEE Trans. Power Syst.*, early access, Jul. 16, 2021, doi: 10.1109/TPWRS.2021.3104905.
[32] B. Liu, J. Zhao, Q. Huang, F. Milano, Y. Zhang, and W. Hu, "Nonlinear virtual inertia control of WTGs for enhancing primary frequency response and suppressing drivetrain torsional oscillations," *IEEE Trans. Power Syst.*, vol. 36, no. 5, pp. 4102–4113, Sep. 2021.
[33] J. Lee, E. Muljadi, P. Srensen, and Y. C. Kang, "Releasable kinetic energy-based inertial control of a DFIG wind power plant," *IEEE Trans. Sustain. Energy*, vol. 7, no. 1, pp. 279–288, Jan. 2016.
[34] W. M. J. Jonkman, S. Butterfield, and G. Scott, "Definition of a 5-MW reference wind turbine for offshore system development," Nat. Renew. Energy Lab., Golden, CO, USA, Tech. Rep., 2009.
[35] D. S. Bernstein, *Matrix Mathematics: Theory, Facts, and Formulas*, 2nd ed. Princeton, NJ, USA: Princeton Univ. Press, 2009. [Online]. Available: http://www.jstor.org/stable/j.ctt7t833
[36] J. Ding and A. Zhou, "Eigenvalues of rank-one updated matrices with some applications," *Appl. Math. Lett.*, vol. 20, no. 12, pp. 1223–1226, 2007. [Online]. Available: https://www.sciencedirect.com/science/article/pii/S0893965907000614

ESTEBAN RIQUELME received the Licenciado, Ingeníero Civil Eléctrica, and Magister degrees in electrical engineering from the University of Santiago, Santiago, Chile, in 2015, 2018, and 2018, respectively, where he is currently pursuing the Ph.D. degree with the Department of Electrical Engineering. He is currently an Instructor with the Department of Electrical Engineering, University of Santiago.

HECTOR CHAVEZ (Member, IEEE) received the Licenciado, Ingeníero Civil Eléctrica, and Magister degrees in electrical engineering from the University of Santiago, Santiago, Chile, in 2004, 2006, and 2006, respectively, and the Ph.D. degree in electrical engineering from The University of Texas at Austin, Austin, TX, USA, in 2013. In 2013, he was a Postdoctoral Fellow with the Department of Electric Power Systems, School of Electrical Engineering, KTH Royal Institute of Technology, Stockholm, Sweden. From 2006 to 2009, he was an Instrumentation Engineer with WorleyParsons Minerals and Metals, Santiago. He is currently an Associate Professor with the Department of Electrical Engineering, University of Santiago.

KARINA ACOSTA BARBOSA (Senior Member, IEEE) received the B.S. degree in mechanical engineering from the National Chung Cheng University, Chiayi, Taiwan, in 2004, and the M.S. degree in mechanical engineering from the National Tsing Hua University, Hsinchu, Taiwan, in 2006. He is currently pursuing the Ph.D. degree in mechanical engineering with Texas A&M University, College Station, TX, USA.

From 2008 to 2009, he was a Research Assistant with the Institute of Physics, Academia Sinica, Tapei, Taiwan. His research interests include the development of surface processing and biological/medical treatment techniques using nonthermal atmospheric pressure plasmas, fundamental study of plasma sources, and fabrication of micro- or nanostructured surfaces.

Mr. Barbosa's awards and honors include the Frew Fellowship (Australian Academy of Science), the I. I. Rabi Prize (APS), the European Frequency and Time Forum Award, the Carl Zeiss Research Award, the William F. Meggers Award, and the Adolph Lomb Medal (OSA).